Supplemental Material

Electron trapping and detrapping in an oxide two-dimensional electron gas: The role of ferroelastic twin walls

Shashank Kumar Ojha, Sankalpa Hazra, Prithwijit Mandal, Ranjan Kumar Patel,
Shivam Nigam, Siddharth Kumar and Srimanta Middey
Department of Physics, Indian Institute of Science, Bengaluru 560012, India

I . Variation of sheet resistance (R_S) under -ve back gate voltage (V_g) sweep:

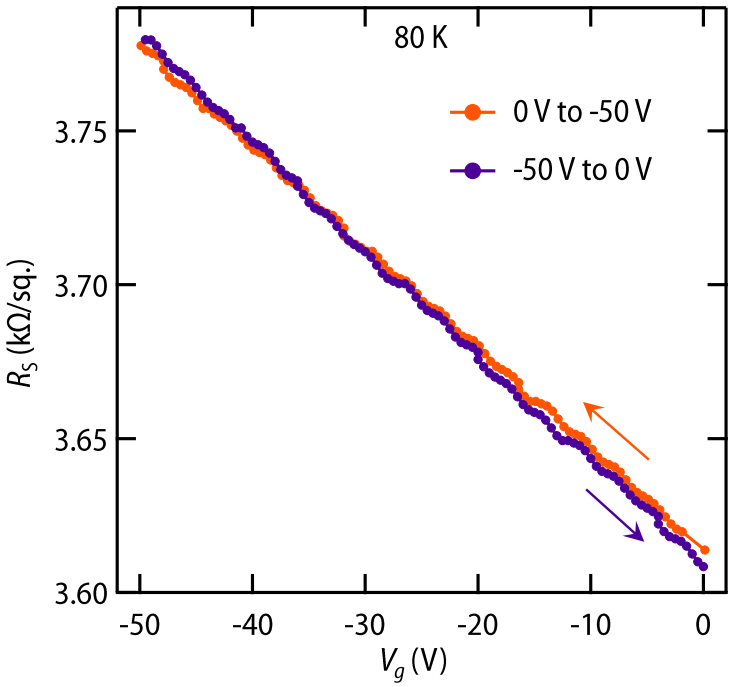

FIG. S1. Variation of R_s when V_g is swept from 0 V $\rightarrow$ -50 V $\rightarrow$ 0 V at 80 K.

To check the presence of any charge trapping/detrapping under -ve back gate voltage, V_g was swept from 0 V $\rightarrow$ -50 V $\rightarrow$ 0 V. As evident from Figure S1, R_S increases with the application of -ve V_g. This arises as -ve V_g removes electrons from the 2DEG. However, no appreciable offset in R_S was observed when V_g was swept backward from -50 V to 0 V, signifying absence of any charge trapping/detrapping under -ve back gate voltage.

Interestingly, the application of -ve step voltage leads to the observation of a detrapping feature C (see Figure 2c in the main text and Figure S2 of this Supporting Information) which can be described by a single exponential decaying function. As shown in the main text, this detrapping feature is completely reversible with electric field and goes away once the electric field is set to zero (also see section X of this Supporting Information).

II. Independent observation of feature C:

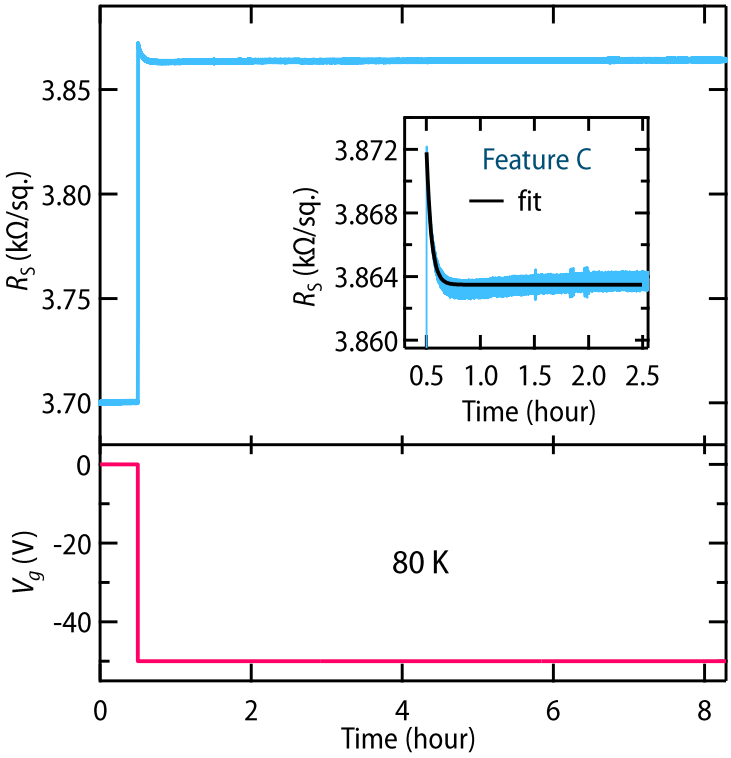

FIG. S2. Observation of feature C by application of a 0 → - 50 V at 80 K. Inset shows the zoomed in view of decaying feature fitted with a single exponentially decaying function with time.

Feature C has also been observed independently by applying a step V_g of - 50 V for roughly 8 hours (Figure S2). We note that the back gating protocol discussed in the main text started with a step voltage of +ve 50 V. Inset of Figure S2 shows feature C fitted with an exponentially decaying function with time for the first 2 hours, yielding a time scale of roughly 150s. This time scale is very similar to what was observed when -ve step voltage was applied after switching off the +ve step voltage (see Figure 2e and gating protocol in the lower panel of Figure 2a of the main text). This implies that the observation of detrapping feature C is independent of any previous gate voltage application.

III. Functional form of feature A:

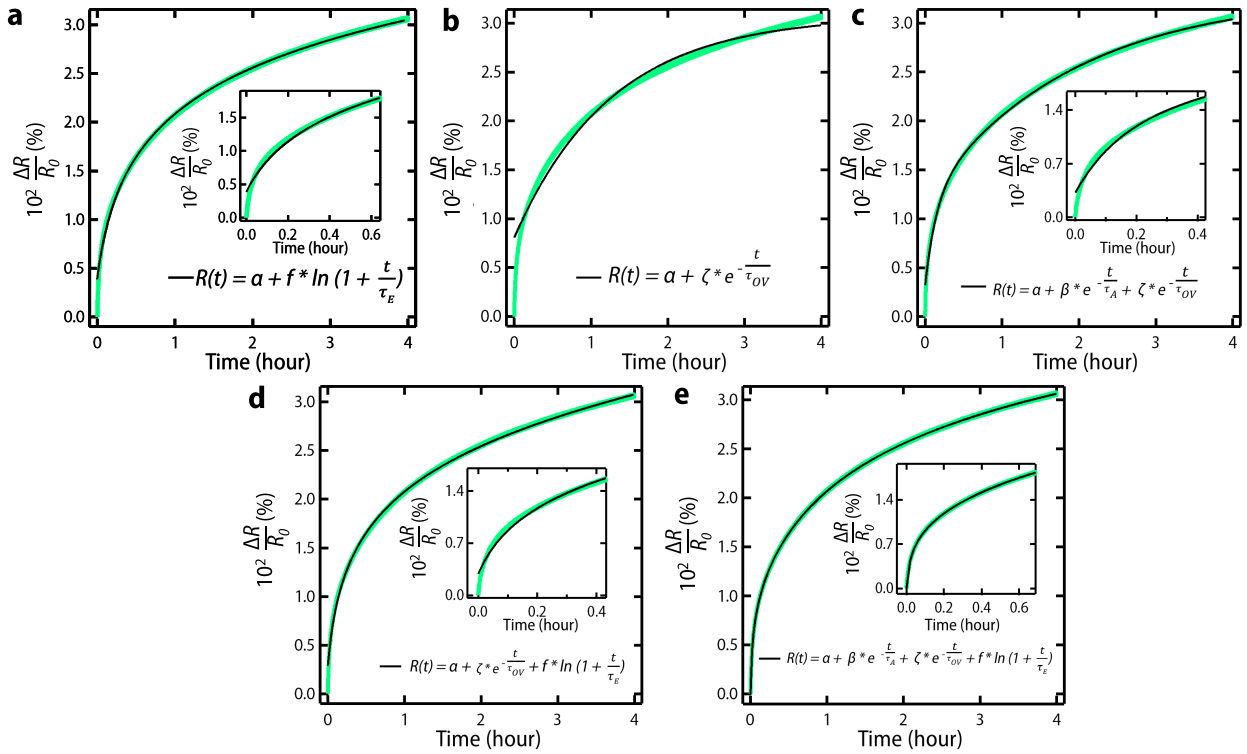

FIG. S3. Fitting of feature A in the 1st cycle at 80 K for V_g=50 V with **a.** thermal escape mechanism. **b.** a single exponentially saturating function. **c.** two exponentially saturating functions. **d.** combination of a single exponentially saturating function and thermal escape contribution. **e.** a combination of two exponentially saturating functions and thermal escape contribution. Insets in figure **a** and **c**-**e** show zoomed sections of the respective fittings near origin for clarity. The corresponding fitting formula has been shown in the inset of each figure. Feature A has been normalized to the first data point.

To describe charge trapping under +ve V_g in our sample, we first used the functional form for thermal escape of electrons from 2DEG under +ve V_g (see inset of Figure S3a for its functional form) as proposed by Biscaras et al [1]. Fitting our data to their proposed functional form does not result in a good fitting (see Figure S3a and its inset). This observation clearly emphasizes that there are additional processes contributing to charge trapping under +ve V_g apart from thermal escape in our sample.

To account for the trapping of electrons in the mid-gap states formed by clustering of OVs, an exponentially saturating function with time has also been used to fit the feature A. This function as well results in a poor fit as shown in Figure S3b. This observation suggests that OV clustering

alone can not account for charge trapping under +ve V_g. We also tried to fit Feature A with two exponential time saturating function, and a combination of one exponential function (for contribution from the clustering of OVs) along with the thermal escape contribution. Both these combinations of fitting functions do not result in a good fitting for feature A, as shown in Figure S3c and S3d respectively.

An excellent fitting is obtained when a combination of two exponentially saturating functions along with thermal escape contribution has been used. Figure S3e and its inset shows an excellent agreement between the data and the fit function. Thus, this combination is the simplest representation of the functional form of feature A. We also note that this particular hybrid function consisting of three mechanisms for charge trapping under +ve V_g and provides an excellent fit to feature A for all the consecutive cycles at 80 K and also at various temperatures and ranges of gate voltages.

The two exponentially saturating functions in feature A can be expressed as $R_\beta - \beta' * e^{-\frac{t}{\tau_A}}$ and $R_\zeta - \zeta' * e^{-\frac{t}{\tau_{OV}}}$ respectively. Here, R_β and R_ζ are offset values of R_S for the two exponential functions, while β' and ζ' are weights of the respective exponential functions. Along with the thermal escape contribution (with an offset of R_f), the hybrid function can be written as below,

$$R = R_0 + (R_\beta - \beta' * e^{-\frac{t}{\tau_A}}) + (R_\zeta - \zeta' * e^{-\frac{t}{\tau_{OV}}}) + (R_f + f * ln(1 + \frac{t}{\tau_E}))$$

$$\implies R = (R_0 + R_\beta + R_\zeta + R_f) + (-\beta' * e^{-\frac{t}{\tau_A}} - \zeta' * e^{-\frac{t}{\tau_{OV}}} + f * ln(1 + \frac{t}{\tau_E}))$$

Defining, the constants $\alpha = R_0 + R_\beta + R_\zeta + R_f$, $\beta = -\beta'$ and $\zeta = -\zeta'$, we arrive at the following expression that we have used to characterise feature A.

$$R = \alpha + \beta * e^{-\frac{t}{\tau_A}} + \zeta * e^{-\frac{t}{\tau_{OV}}} + f * ln(1 + \frac{t}{\tau_E})$$

As expected, the fitting of feature A reveals negative values for the terms β and ζ. In contrast, feature B, C and D are fitted to one exponential functions of the form, $a + b * e^{\frac{-(t-t_0)}{\tau_X}}$ (X = features B, C or D). The term b is positive for feature B and C, while it is negative for feature D.

IV. Cycle dependence of OV cluster contribution and additional charge trapping contribution to feature A:

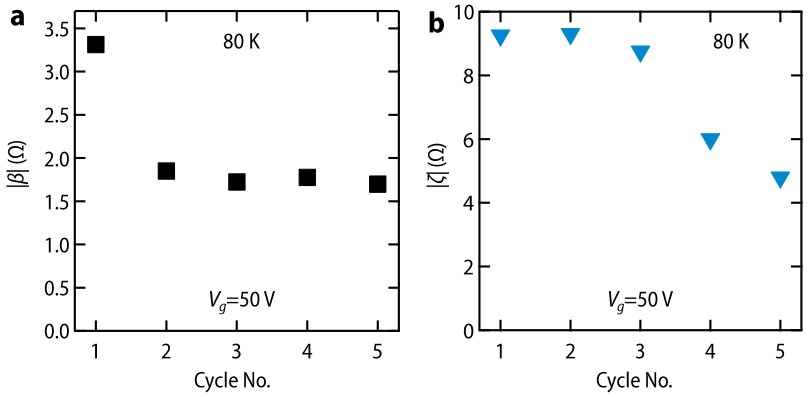

FIG. S4. Cycle dependence of $|\beta|$ and $|\zeta|$ at 80 K for V_g= 50V has been shown in panel **a** and **b** respectively.

To understand the cycle dependence of the additional charge trapping contribution to feature A, we plot the coefficient ($|\beta|$) of the exponential function that accounts for this mechanism with increasing number of cycles in the Figure S4a. As evident $|\beta|$ does not change much at higher cycles. This can be attributed to completely reversible nature of this charge trapping mechanism once the electric field is switched off (see section X of Supporting Information).

In contrast to $|\beta|$, the coefficient ($|\zeta|$) of the exponential function denoting clustering of OVs decreases gradually after the 2nd cycle (Figure S4b), indicating that the OV cluster contribution decreases with increasing cycles. This happens because, after each cycle the concentration of isolated OVs decreases due to the formation of new OV clusters at each cycle. This would lead to a lesser number of new OV clusters formed in the next cycle and is the microscopic reason behind the decreasing trend of OV cluster contribution with increasing number of cycles (see next section).

V. Electric field induced clustering of oxygen vacancies and its redistribution during a complete voltage cycle:

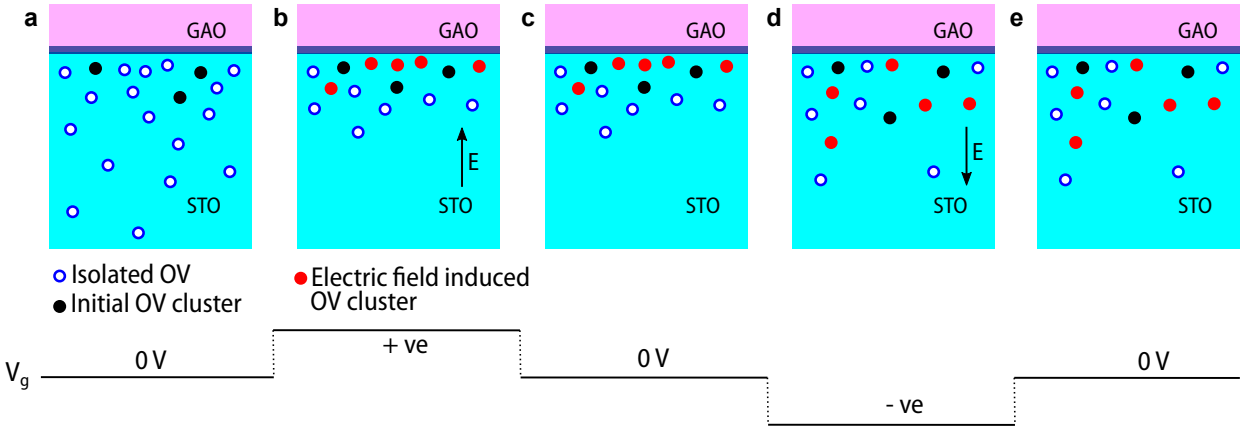

FIG. S5. **a.** Schematic to show isolated OVs and initial OV clusters in STO at zero electric field. **b.** Formation of field induced OV clusters under +ve V_g. **c** Isolated OVs and OV clusters when V_g is switched to zero. **d.** Redistribution of isolated OV and OV clusters under -ve V_g. **e.** Final distribution of isolated OV and OV clusters when V_g is switched to zero. Arrows in figure **b** and **d** denote the electric field direction inside STO.

Under thermal equilibrium at zero electric field, STO of the GAO/STO heterostructure has isolated oxygen vacancies (OVs) and a few initial OV clusters (Figure S5a). Since the 2DEG in GAO/STO emerges from the formation of OVs, the concentration of OVs would be higher at the interface than the bulk of the STO. When a +ve gate voltage (V_g) is applied, the positively charged isolated OVs migrate towards the 2DEG [2]. Due to the high concentration of OVs near the 2DEG, the migrated OVs give rise to new electric field induced OV clusters near the interface (Figure S5b). The new OV clusters give rise to mid-gap states within the band gap of STO, which traps electrons from the 2DEG. Removing the +ve V_g does not alter the OV distribution profile (Figure S5c). When a -ve V_g is applied the isolated OVs and the OV clusters move away from the interface towards bulk of the STO, as shown in Figure S5d. Due to very little concentration of OVs in the bulk of STO, almost no new OV clusters will be formed under -ve V_g. Even if there is any formation of a small number of new OV clusters it will be swept away from the 2DEG and cannot trap any free carrier from the 2DEG. This explains the absence of any OV clustering contribution to charge trapping under -ve V_g. When the V_g is turned to zero the number of isolated OVs finally present is lesser in concentration than in the initial unbiased condition (Figure S5e).

VI. Cycle dependence of feature A:

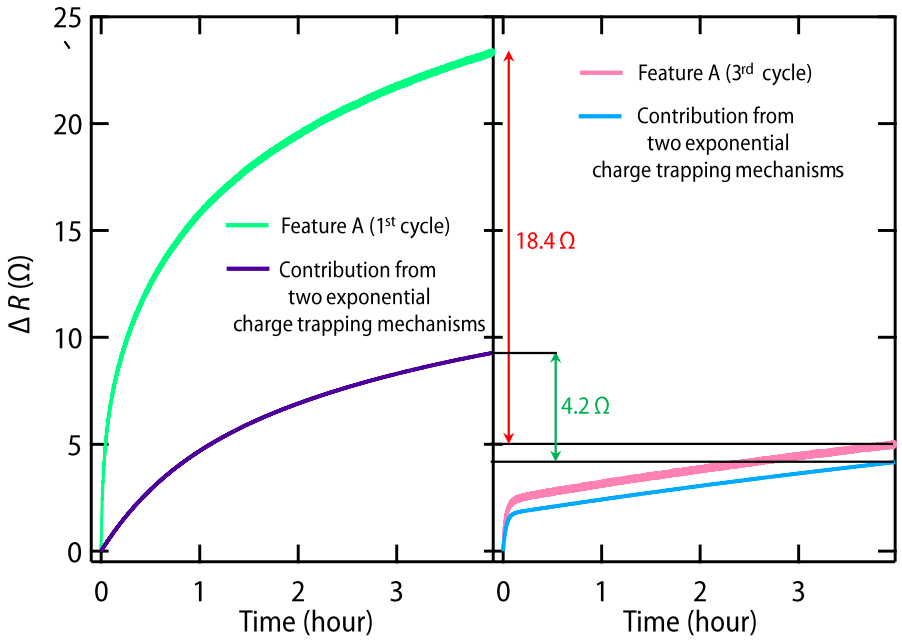

FIG. S6. Change in resistance ΔR due to charge trapping feature A along with two exponential charge trapping mechanisms contributing together to feature A at 80 K for V_g=50 V in the 1st and 3rd cycle has been shown in the left and the right panel respectively.

As shown in the above figure, the net drop in resistance due to feature A from 1st to 3rd cycle at the end of 4 hours (marked by the red arrow) is around 18.4 ohm, whereas the combination of two exponential charge trapping mechanisms contributing to feature A, defined by β*e$^{-\frac{t}{\tau_A}}$ + ζ*e$^{-\frac{t}{\tau_{OV}}}$ - (β+ζ), can only account for 4.2 ohm decrease (marked by the green arrow). This would mean that the combination of the two exponential processes can only account for 22 percent of the net drop in resistance due to feature A from 1st to 3rd cycle and the rest 78 percent is attributed to thermal escape contribution.

VII. Temperature dependence of feature A:

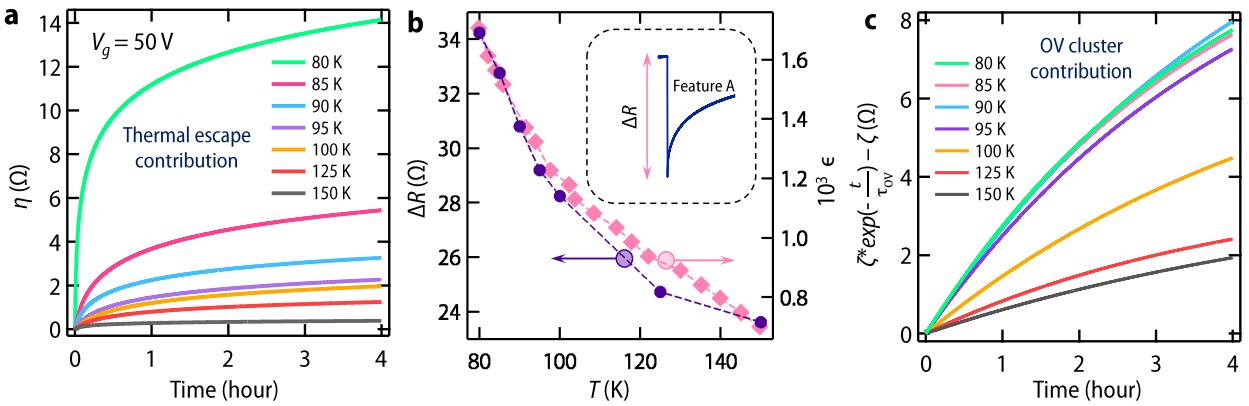

FIG. S7. **a** Temperature dependence of thermal escape contribution to charge trapping under +ve V_g. **b** Temperature dependence of change in resistance ΔR just after the application of +ve step voltage in the first cycle (left axis) and dielectric constant ϵ (right axis). ϵ has been taken from ref [3]. **c** Temperature variation of OV cluster contribution to charge trapping.

To understand the microscopic origin behind the vanishing of feature A above 150 K, all the three processes contributing to feature A have been analyzed separately. For further discussion, we only concentrate on the temperature evolution of thermal escape and OV clustering contributions as the other additional charge trapping process does not survive above 100 K (also see Figure 4 of main text).

We first discuss the temperature evolution of the thermal escape contribution. As evident from Figure S7a, the thermal escape contribution (η) decreases with the increase of T and vanishes above 150 K. Since, the probability of thermal escape is controlled by the position of the Fermi level with respect to the top of the quantum well (see Figure 3(b) of main text), we plot the drop in resistance (ΔR, see inset of Figure S7b) just after the application of first +ve step voltage in the first cycle as a function of T in the Figure S7b. ΔR is directly proportional to the amount of induced charge at the interface (Δn=$\frac{C_a V_g}{e}$ where C_a is the capacitance per unit area of STO and e is the electrons charge) by the application of V_g and is a direct measure of the amount of doping through back gating. As evident, ΔR not only decreases with the increase of T but also smoothly scales with the dielectric constant (ϵ) of STO as expected (C_a=ϵ/l for a parallel plate capacitor with plate separation distance l). This observation implies that the Fermi level (just after application of +ve step voltage) goes deeper with increasing T, which in turn would increase the barrier height ΔE_{barr} (see Fig. 3(b) of main text) for thermal escape, hence reducing the thermal

escape probability with increasing temperature.

The contribution from OV cluster, defined by ζ*exp(-$\frac{t}{\tau_{\mathrm{OV}}}$) - ζ, also decreases with T (Figure S7c). This is obvious as increasing the temperature would thermally depopulate the mid-gap states formed due to OV clusters. We note that at similar temperature ($\sim$ 160 K), intrinsic traps in LAO/STO system have also been found to disappear[4].

VIII. Temperature dependence of feature C and D:

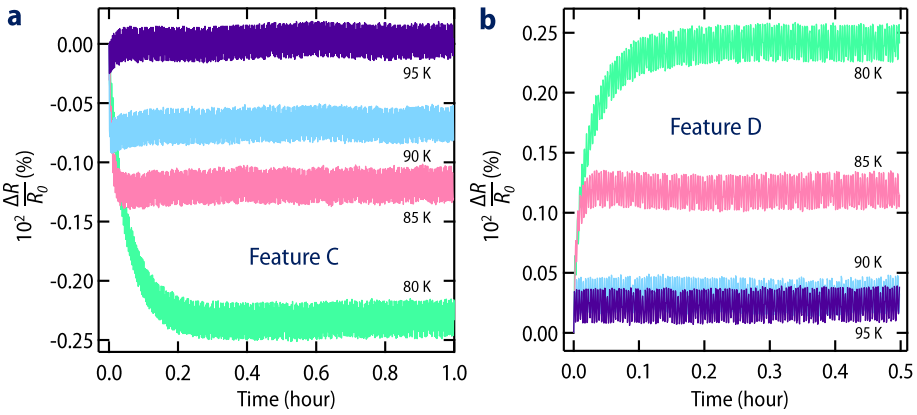

FIG. S8. Temperature dependence of relative percentage change in resistance ($10^2 \frac{\Delta R}{R_0}$) due to detrapping feature C (1st cycle) and trapping feature D (1st cycle) have been shown in panel **a** and **b** respectively.

Similar to the temperature dependence of additional charge trapping contribution to feature A, feature B, features C (Figure S8a) and D (Figure S8b) also vanishes above 100 K. This observation again points to a common microscopic origin behind the observation of additional charge trapping contribution to feature A and features B, C and D.

IX. Temperature dependence of additional charge trapping contribution to feature A and feature B in the 2nd and 3rd cycle:

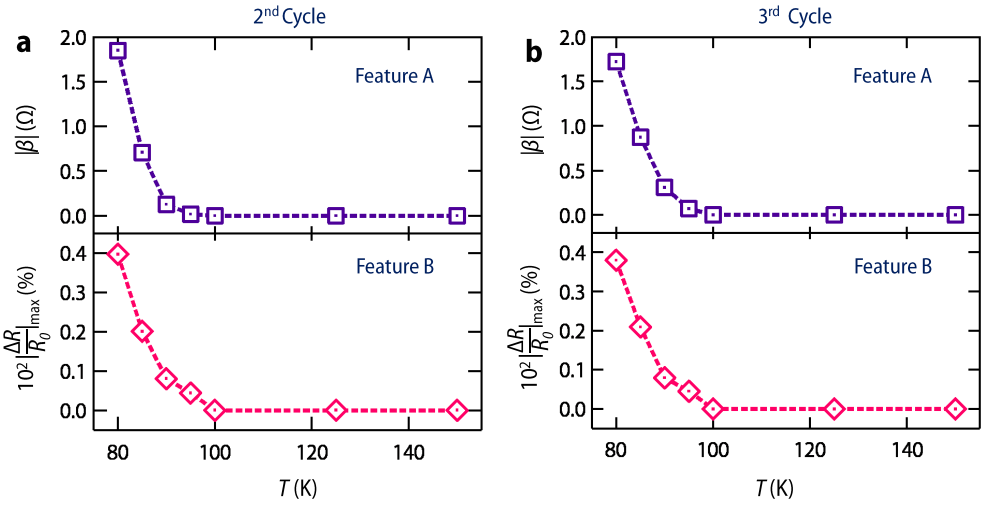

FIG. S9. Temperature evolution of $|\beta|$ obtained from fitting of feature A (upper panel) and magnitude of the maximum relative percentage change in resistance (10^2 $|\frac{\Delta R}{R_0}|_{\max}$) due to detrapping feature B (lower panel) in the 2nd and 3rd cycle has been shown in panel **a** and **b** respectively.

Figure S9a shows the temperature evolution of $|\beta|$ obtained from fitting of feature A (2nd cycle) and magnitude of the maximum relative percentage change in resistance (10^2 $|\frac{\Delta R}{R_0}|_{\max}$) due to detrapping feature B (2nd cycle) in the upper and lower panel respectively. As clearly seen, both of them vanishes above 100 K. Similar temperature dependence has been observed in the 3rd cycle as well (see panel b of Figure S9).

X. Reversible nature of additional charge trapping contribution to feature A under +ve V_g and charge detrapping under -ve V_g:

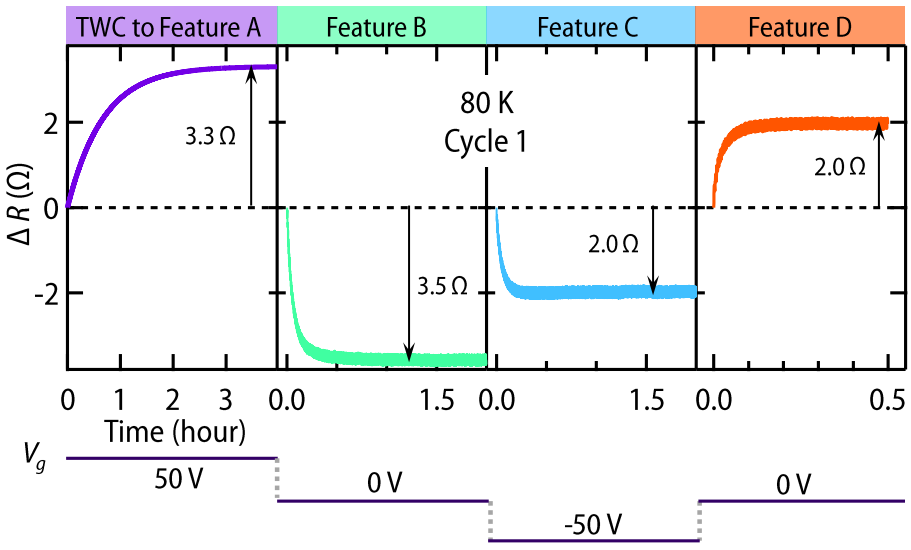

FIG. S10. Change in resistance (ΔR) due to additional charge trapping contribution (β*e$^{-\frac{t}{\tau_A}}$-β) to feature A and features B, C and D at 80 K in the first voltage cycle for the maximum applied V_g= 50V.

The OV cluster contribution and the thermal escape contribution to feature A do not reverse back upon switching off the +ve back gate voltage. However, the additional charge trapping contribution (β*e$^{-\frac{t}{\tau_A}}$-β) to feature A is seen to be completely reversible upon removing the applied positive V$_g$. This is evident from Figure S10 where we plot the change in resistance ΔR due to the additional charge trapping contribution to feature A and feature B together at 80 K in the first cycle. The maximum change in resistance (ΔR_{max}) due to the additional charge trapping contribution to feature A comes out to be around 3.3 Ω (1$^{\text{st}}$ panel of Figure S10). Switching off the voltage leads to the detrapping feature B. ΔR_{max} corresponding to feature B comes out to be 3.5 Ω (2$^{\text{nd}}$ panel of Figure S10). The nearness of the two values indicates that the additional charge trapping contribution to feature A is completely reversed when V_g is brought to zero.

Further, detrapping of carriers under application of -ve V_g (feature C) is also found to be completely reversible. This is evident from ΔR_{max} for features C and D shown in the 3$^{\text{rd}}$ and the 4$^{\text{th}}$ panel of Figure S10. We also note that the additional charge trapping contribution to feature A under +ve V_g and charge detrapping under -ve V_g is found to be reversible in the successive cycles as well (Figure S11).

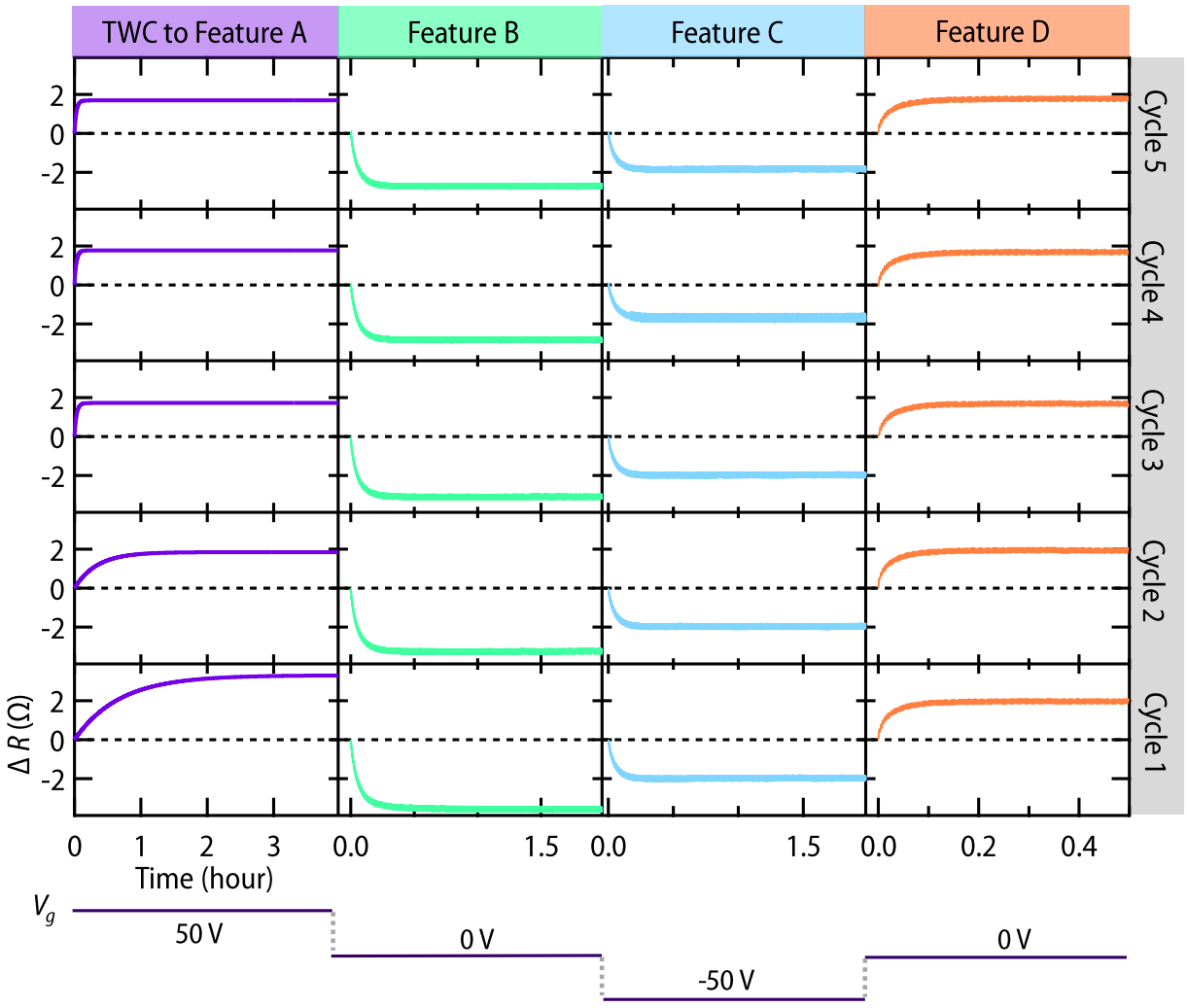

FIG. S11. Cycle dependence of change in resistance (ΔR) due to additional charge trapping contribution (β*e$^{-\frac{t}{\tau_A}}$-β) to feature A and features B, C and D at 80 K for maximum applied V_g= 50V.

XI. Effect of electric field strength on charge trapping under +ve V_g:

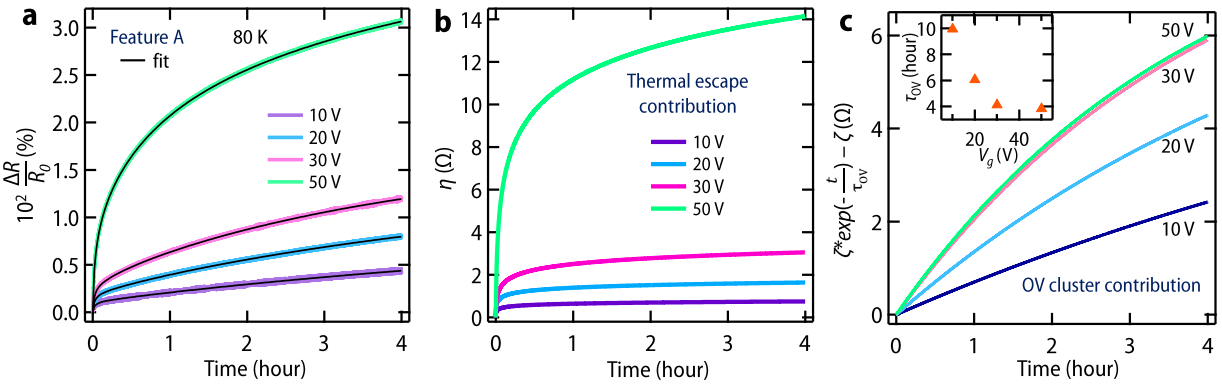

FIG. S12. **a.** Time evolution of feature A (1st cycle) with increasing V_g at 80 K. **b.** V_g dependence of thermal escape contribution. **c.** V_g dependence of OV cluster contribution, inset shows the V_g dependence of τ_{OV} .

To study the role of electric field strength on charge trapping under +ve V_g, voltage dependent measurements have been performed. Figure S12a shows the variation of feature A (1st cycle) with increasing V_g at 80 K. As evident, it increases with increasing V_g. For further understanding, individual contributions to feature A have been analyzed. Thermal escape contribution shows an increasing trend with increasing field (Figure S12b). This is expected, as increasing the electric field will lead to more band bending, leading to the lowering of ΔE_{barr} for thermal escape. This will eventually make the thermal escape easier and explains the enhancement of thermal escape contribution with increasing field.

OV cluster contribution also shows an enhancement with increasing field (Figure S12c). To better understand this, we plot τ_{OV} vs V_g in the inset of Figure S12c. As evident, τ_{OV} decreases with increase in the electric field. This would mean that, at higher fields, it would take lesser time for the formation of OV clusters. Certainly, for a given amount of time, more OV clusters would be formed at the higher field and hence OV cluster contribution would show an enhancement with increasing electric field.

XII. Additional data on another 15 unit cell γ-Al_2O_3/$SrTiO_3$ sample:

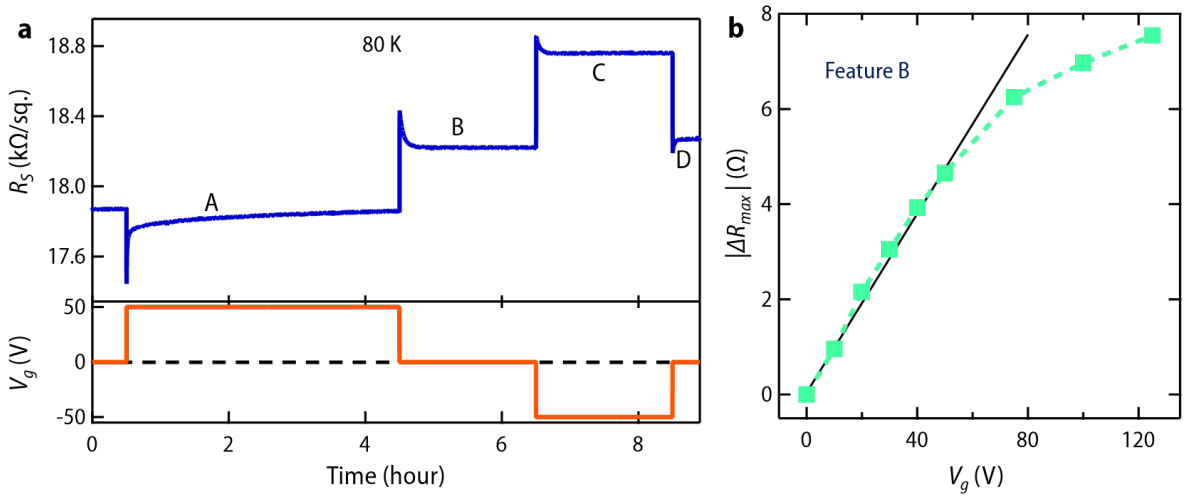

FIG. S13. **a.** Variation of sheet resistance with applied back gate protocol for 1st cycle at 80 K. **b.** Variation of magnitude of maximum change in resistance due to detrapping feature B in the 1st cycle at 80 K with increasing $V_g^{\max}$.

Upper panel of Fig. S13a shows the representative plot of variation of R_S with applied back gate protocol for 1st cycle at 80 K for another sample with similar thickness. As observed for the other sample, all the features A, B, C and D are very prominent. Fig. S13b shows the variation of the magnitude of maximum change in resistance due to detrapping feature B in the 1st cycle at 80 K with increasing $V_g^{\max}$ upto 125 V. As evident it varies linearly upto 50 V (this behavior is similar to the sample discussed in the main text) but becomes non-linear above that. Such saturating trend at higher V_g might arise from the fact that with increasing V_g more electrons are attracted towards the twin wall. These excess electrons would screen the local electric field around the twin wall, preventing further charge accumulation.

[1] J. Biscaras, S. Hurand, C. Feuillet-Palma, A. Rastogi, R. Budhani, N. Reyren, E. Lesne, J. Lesueur, and N. Bergeal, Scientific reports **4**, 6788 (2014).

[2] C. Yin, A. E. Smink, I. Leermakers, L. M. Tang, N. Lebedev, U. Zeitler, W. G. van der Wiel, H. Hilgenkamp, and J. Aarts, Physical Review Letters **124**, 017702 (2020).

[3] T. Sakudo and H. Unoki, Phys. Rev. Lett. **26**, 851 (1971).

[4] S. Seri, M. Schultz, and L. Klein, Phys. Rev. B **87**, 125110 (2013).